APPLIED PHYSICS LETTERS **104**, 203506 (2014)

Growth-substrate induced performance degradation in chemically synthesized monolayer MoS_2 field effect transistors

Matin Amani,[1] Matthew L. Chin,[1] Alexander L. Mazzoni,[1] Robert A. Burke,[1] Sina Najmaei,[2] Pulickel M. Ajayan,[2] Jun Lou,[2] and Madan Dubey[1,a)]

[1]*Sensors and Electron Devices Directorate, US Army Research Laboratory, Adelphi, Maryland 20723, USA*
[2]*Department of Materials Science and Nanoengineering, Rice University, Houston, Texas 77005, USA*

(Received 20 February 2014; accepted 13 April 2014; published online 23 May 2014)

We report on the electronic transport properties of single-layer thick chemical vapor deposition (CVD) grown molybdenum disulfide (MoS_2) field-effect transistors (FETs) on Si/SiO_2 substrates. MoS_2 has been extensively investigated for the past two years as a potential semiconductor analogue to graphene. To date, MoS_2 samples prepared via mechanical exfoliation have demonstrated field-effect mobility values which are significantly higher than that of CVD-grown MoS_2. In this study, we will show that the intrinsic electronic performance of CVD-grown MoS_2 is equal or superior to that of exfoliated material and has been possibly masked by a combination of interfacial contamination on the growth substrate and residual tensile strain resulting from the high-temperature growth process. We are able to quantify this strain in the as-grown material using pre- and post-transfer metrology and microscopy of the same crystals. Moreover, temperature-dependent electrical measurements made on as-grown and transferred MoS_2 devices following an identical fabrication process demonstrate the improvement in field-effect mobility. © *2014 AIP Publishing LLC*.
[http://dx.doi.org/10.1063/1.4873680]

Two-dimensional (2D) materials have become a topic of very intense research since the isolation of single graphene layers by mechanical exfoliation in 2004 and have recently expanded beyond graphene to include superconducting, semiconducting, and insulating materials.[1,2] In conjunction with newly identified members of the 2D material family, innovative ideas for device modalities such as valleytronics as well as stacked heterostructures have been identified and realized through aligned exfoliation techniques.[3–5] The prototypical semiconducting 2D material currently being investigated by a large fraction of the 2D research community is molybdenum disulfide (MoS_2). MoS_2 is a layered dichalcogenide which exhibits an indirect-to-direct bandgap transition as it is thinned down from a bilayer to a monolayer.[6] In addition to this shift in band-structure, the inversion symmetry of the monolayer MoS_2 crystal is lost, resulting in numerous interesting properties such as piezoelectricity and strong spin-orbit interaction, which could be utilized in future electro-mechanical/optical systems.[7,8] MoS_2 shows promise as a material for high-performance, low-power logic devices, which can be easily modified for flexible electronics applications.[3,9–12] Additionally, encapsulation of MoS_2 in a high-κ dielectric such as HfO_2 or Al_2O_3 has been shown to dramatically improve both the field-effect mobility and on/off current ratios through screening effects and reduced phonon scattering, although the magnitude of this effect was overestimated in early studies.[13–15] Moreover, recent theoretical studies on strain engineering as well as the effect of interfacial impurities on two dimensional lattices can dramatically alter the materials band-structure as well as reduce the mobility by as much as several orders of magnitude.[16,17]

Initial material characterization and device research on MoS_2 and other 2D materials have typically been accomplished through the use of exfoliated films. In parallel to the discoveries made on exfoliated samples, there have been efforts in the growth community to synthesize large-area sheets of these 2D materials, which can either be transferred to a desired substrate or directly grown on a wide variety of target substrates.[18–20] Chemical vapor deposition (CVD) of graphene on copper foils has gained the most traction of these efforts and has recently demonstrated both centimeter-scale single--crystals, as well as growth on 30 in. foils. These two key achievements have made the performance of CVD graphene comparable to exfoliated samples and have demonstrated that graphene can be readily scaled for commercial production.[21,22] The growth of MoS_2 utilizing CVD is a much more recent endeavor and has predominantly been carried out using powder precursors and directly grown on dielectric substrates (most commonly Si/SiO_2). This has been incredibly convenient for device fabrication, as it cuts out the transfer step required for graphene grown on Cu foils. The transfer step has frequently caused fabrication difficulties due to contamination and doping of the graphene film from the metal etchants and the poly (methyl methacrylate) (PMMA) protective layer as well as tears and folds resulting from handling during the transfer.[23] Metrology of CVD-grown MoS_2 by Raman, photoluminescence (PL), and annular dark-field scanning transmission electron microscopy (ADF-STEM) has shown that the films are typically of very high quality comparable to exfoliated materials.[18] However, the electrical performance of field-effect transistors (FETs) built on unpassivated, monolayer, CVD-grown MoS_2 has been approximately an order of magnitude lower than exfoliated materials, although significant variation is observed depending on growth conditions, sample geometry, etc.[13,18,19,24–27] In this manuscript, we fabricate three sets of devices using an identical process flow with

a)Author to whom correspondence should be addressed. E-mail: madan.dubey.civ@mail.mil

 © 2014 AIP Publishing LLC

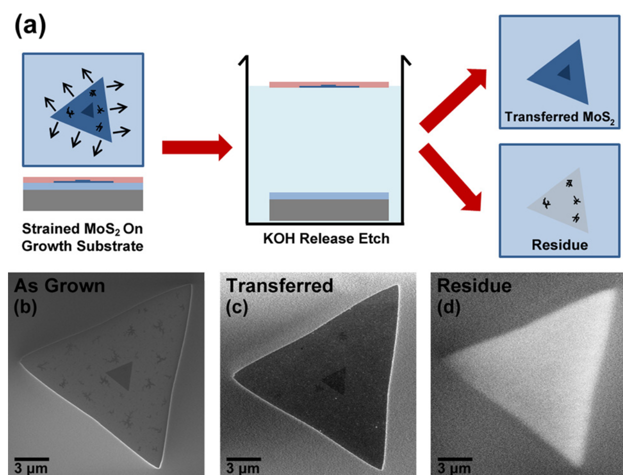

FIG. 1. Schematic showing the transfer process (a). Secondary electron SEM images taken of the same MoS_2 crystal taken both before (b) and after (c) transfer as well as of the residual surface contamination left on the surface of the growth substrate after removal from the etchant solution (d).

monolayer MoS_2 channels based on: (1) micromechanically exfoliated MoS_2 on a Si/SiO_2 substrate, (2) CVD MoS_2 on the growth Si/SiO_2 substrate, and (3) CVD MoS_2 transferred to an identical Si/SiO_2 substrate. We show that contamination at the MoS_2/SiO_2 interface resulting from the growth process as well as residual tensile strain on the original substrate limit device performance of the as-grown material. However, by transferring MoS_2 to a new, identical substrate and removing these factors, we are able to obtain superior mobility and on/off ratio relative to exfoliated films.

Monolayer MoS_2 films were grown directly on a 285 nm SiO_2/Si substrate using the procedure described in detail by Najmaei *et al.*[18] Several samples were transferred from their original growth substrate. A PMMA layer was spin coated on these samples and allowed to dry at room temperature overnight. The MoS_2 samples were then transferred from the growth Si/SiO_2 substrates onto new substrates with identical oxide thickness using a 0.2 M KOH solution heated to 60 °C for the release etch. Typically, a total etch time of 1.5–2 h was required. A schematic of the transfer procedure is shown in Figure 1(a). In addition, we fabricated devices on mechanically exfoliated monolayer MoS_2 (SPI Supplies) prepared using the scotch tape method.[34–36] All devices were fabricated with electron-beam lithography (EBL) using a MMA/PMMA bilayer resist process for all steps. The MoS_2 layer was patterned using a low-power reactive ion etch in a CH_4/O_2 plasma, and source and drain contacts were made using e-beam evaporated Ti/Au (15/85 nm).

We characterized the MoS_2 at various stages during processing using high-resolution Raman and PL imaging. These measurements were performed with a WITec Alpha 300RA system using the 532 nm line of a frequency-doubled Nd:YAG laser as the excitation source. The spectra were measured in the backscattering configuration using a 100× objective and either a 600 or 1800 grooves/mm grating for PL and Raman, respectively. The spot size of the laser was ~342 nm resulting in an incident laser power density of $\sim 140\,\mu W/\mu m^2$. This power level was chosen such that no time-dependent shifting of the E_{2g} and A_{1g} modes was produced during the measurement. Scanning electron microscopy (SEM) was used to characterize the changes in morphology of the films; however, due to potential damage by the electron beam,[36] these devices were not used in subsequent metrology or for device fabrication. All electrical measurements were obtained using a Keithley 4200 parameter analyzer with the substrate as a universal back gate. Measurements were taken from 77 K to 350 K at a pressure no greater than 2×10^{-6} Torr.[24] A source drain voltage of 500 mV was used for all two-point measurements and four-point measurements were performed with a voltage bias of 1 V on the outer probes (resulting in no more than 600 mV across the channel due to the voltage drop at the contacts). Prior to testing the samples, they were annealed in vacuum at 400 K using the procedure described by Baugher *et al.*[37] to improve the device contact resistance and linearity. After the transferred sample was characterized, a 15 nm Al_2O_3 layer was grown on the samples using atomic layer deposition (ALD) performed at 170 °C and the measurements were repeated to show the reduction in Coulomb scattering caused by the high-κ dielectric.[17,38]

In order to investigate and understand the physical effects of the substrate on the MoS_2 growth, we imaged several single crystal flakes on the growth substrate and subsequently identified and imaged the same flakes after transferring to a new substrate. Secondary electron images of an original and transferred crystal grain are shown in Figures 1(b) and 1(c). By carefully measuring the average change in the side lengths of the same MoS_2 triangles both before and after transfer, we were able to determine that the MoS_2 flakes were under a residual tensile strain of 1.24% on the growth substrate, which was effectively released after the flakes were transferred to a new substrate. We believe that the strain is caused when the sample is cooled after growth and is a by-product of the thermal coefficient of expansion mismatch between MoS_2 and SiO_2/Si. Additionally, we examined the original growth substrate to identify any residue left behind after the MoS_2 was transferred (Figure 1(d)). We can also observe a dramatic reduction in density of the dendrite like structures observed in the as grown sample after transfer. Imaging of the original substrate showed that there was residual contamination in the original location and shape of the MoS_2 films. It is likely caused by non-carbon based contamination which forms during the growth process; further details can be found in the supplementary material.[39] The residue is also believed to account for the inaccurate AFM step-height measurements of CVD-grown material that have been previously reported.[24]

To study the optical and structural variations and verify the tensile strain measured in the as-grown MoS_2, high-resolution Raman and PL mapping were performed on the same chemically synthesized single-crystal both before and after transfer. The results were subsequently compared to a high-quality monolayer flake prepared by mechanical exfoliation; Raman and PL mapping of the exfoliated monolayer sample is shown in supplementary Figure S2.[39] Single Raman spectra taken for each sample are shown in Figure 2(a) and critical parameters from the in-plane (E^1_{2g}) and out-of plane (A_{1g}) vibrational modes have been extracted and are shown in Table I. Utilizing the Grüneisen parameter, experimentally measured from Refs. 28 and 29 and assuming that the strain in the MoS_2 is fully released after transfer, we can attribute the shift in the E^1_{2g} peak by 2.799 cm^{-1} and the A_{1g} peak by

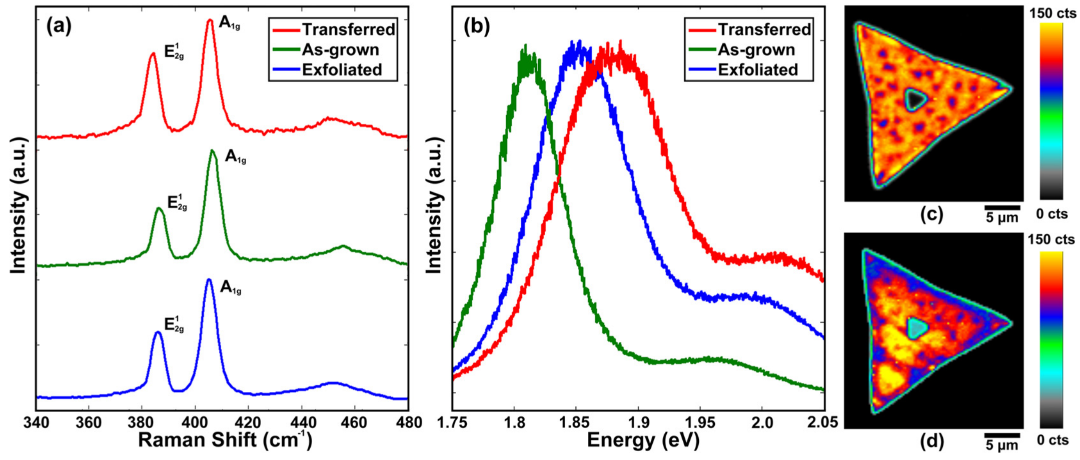

FIG. 2. Normalized Raman (a) and PL (b) spectra obtained for exfoliated, as-grown CVD, and transferred CVD monolayer MoS_2. PL mapping of the same MoS_2 crystal taken both before (c) and after (d) transfer, showing the relaxation of reduced intensity PL spots resulting from the growth process.

$0.566\,cm^{-1}$ to a 1.37% tensile strain in the as-grown material. This is in good agreement with the value extracted from the SEM images and can likely be attributed for growth-to-growth process variation. In addition to the relative shift in peak positions, we also found that the intensity ratio of the $E^1{}_{2g}/A_{1g}$ modes in the CVD material, which is also listed in Table I, approaches that of the exfoliated sample after transfer.[27,29]

As expected for semiconductors under tensile strain and in good agreement with band structure simulations for MoS_2,[28] the A-exciton (X^0) of the as-grown MoS_2 (Figure 2(b)) is red-shifted relative to the transferred material by 68 meV with little to no loss of intensity and is accompanied by an increase in the full-width-half-maximum of the peak. The latter can potentially be explained by n-type doping of the material as a result of the transfer processes, which can increase the intensity of the negatively charged trion (X^-) peak.[30] Since the trion (X^-) peak typically has a binding energy of only 40 meV below that of the exciton (X^0) peak, an apparent widening of the PL is typically observed at room temperature, and cryogenic measurements are required to resolve the separate signals.[31] This hypothesis is further supported by the increase in carrier density after the transfer, which is measured from back-gated FETs. The experimental values are shown in Table I and will be discussed in more detail below. We are able to track the change in intensity of the synthesized MoS_2 with high-resolution PL mapping, as shown in Figures 2(c) and 2(d), for the same MoS_2 triangle both before and after transfer. Several regions of reduced intensity (∼15% quenching) can be seen in the MoS_2 before being transferred and are partially removed in the map taken after transfer.

Back-gated FETs were constructed for the three different MoS_2 sample sets using identical Ti/Au contacts and lithography procedures. Devices with varying length (L) and width (W) ratios were fabricated in order to extract contact resistance using the transmission line measurement (TLM), and structures for four-point probe measurements were made to extract the impact of contact resistance from the data. Optical micrographs showing examples of the fabricated devices are shown in supplementary Figure S3.[39] The I_{DS}-V_{GS} characteristics of monolayer MoS_2 transistors taken at a 500 mV drain bias with an L/W of 1/1 μm are shown in Figures 3(a) and 3(b) at both room temperature and 77 K, respectively. Similar measurements showing channel conductance (G_{DS}) taken using the four-point probe method are shown in Figure 3(c). We extracted the field effect mobility in these samples using the following equation:

$$\mu_{2PP} = \frac{dI_{DS}}{dV_{BG}} \times \frac{L}{WC_g V_{DS}}, \tag{1}$$

where C_g is the gate capacitance per unit area, L is the channel length, W is the channel width, V_{DS} is the drain-source voltage, and $\frac{dI_{DS}}{dV_{BG}}$ is the slope of the I_{DS}-V_{GS} characteristics taken in the linear region. In the case of four-point measurements, the channel conductivity is used to calculate mobility based on

$$\mu_{4PP} = \frac{d\sigma}{dV_{BG}} \times \frac{L}{WC_g}, \tag{2}$$

where $\frac{d\sigma}{dV_{BG}}$ is the slope of the conductance with respect to gate voltage taken in the linear region.

For our exfoliated device, we measured two- and four-point mobility values of 8.93 and 16.27 cm^2/V s, respectively, which is within the range of what has been previously reported in the literature for similarly scaled exfoliated devices.[14] On the other hand, as-grown monolayer FETs showed two- and four-point mobility values of 2.26 and 5.02 cm^2/V s. This falls within the wide range of values typically

TABLE I. Key Raman parameters, room temperature field effect mobility, and carrier density for exfoliated, as-grown, and transferred monolayer MoS_2 samples.

	ω_{E2g} (cm^{-1})	ω_{A1g} (cm^{-1})	$\Delta\omega$ (cm^{-1})	I_{A1g}/I_{E2g}	$\mu_{FE,4PP}$ (cm^2/V s)	N_D (cm^{-2})
Exfoliated	386.191	405.346	19.155	1.807	16.27	2.7×10^{12}
CVD as-grown	386.792	405.875	22.270	1.365	5.02	2.0×10^{12}
CVD transferred	386.591	406.441	19.849	1.844	17.63	4.9×10^{12}

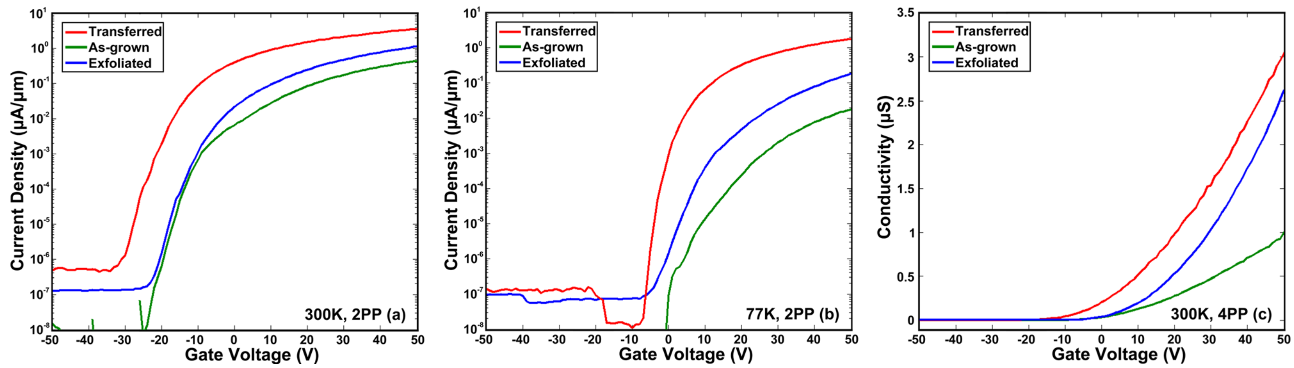

FIG. 3. I_{DS}-V_{GS} characteristics of as-grown, transferred, and exfoliated monolayer MoS_2 taken at $V_{DS} = 500$ mV and 300 K (a) or 77 K (b) from two-point measurements. Room temperature G_{DS}-V_{GS} characteristics at room temperature from four-point measurements (c).

reported, which have much greater variability than exfoliated devices. Variation in the reported field effect mobility has ranged from as low as 0.003 cm^2/V s to as high as 10 cm^2/V s, depending heavily on growth conditions, device/contact geometry, and fabrication processes.[13,18,19,24–27] Finally, for the transferred devices, the two- and four-point mobility values increase to 15.06 and 17.63 cm^2/V s, respectively. These values are significantly higher than the exfoliated devices measured in this study, and simultaneously show a dramatic improvement in the on-currents for FETs, which is a major concern for deeply scaled monolayer devices.[32] It is important to note that the difference between the four and two point mobility values is primarily determined by contribution from the contact resistance, which varies for each of the device sets (at $V_{bg} = 50$ V, we find $\rho_c \sim 6$ Ω mm, $\rho_c \sim 8.5$ Ω mm, and $\rho_c \sim 2.8$ Ω mm for exfoliated, as grown, and transferred MoS_2, respectively). The intrinsic carrier concentration for the three devices was calculated using $N_D = C_g \cdot V_{Th}/e$, where V_{Th} is the threshold voltage and e is the elementary charge. The results (Table I) show that the transfer process leads to a significant n-type doping of the material, which are consistent with a broadening of the PL resulting from a combined exciton and negatively charged trion peak as shown in Figure 2(b).

To further explore the transport properties of the transferred MoS_2 device, we performed detailed temperature-dependent transport measurements with no passivation as well as with an ALD Al_2O_3 passivation which is shown in Figures 4(a) and 4(b). Room temperature I_{DS}-V_{DS} sweeps are shown in the inset plots in Figure 4. As would be expected based on previous reports, a relative improvement in the field effect mobility was observed by a factor of ∼2.6 due to the presence of a high-κ coating, coupled with a strong negative shift in the threshold voltage. From these measurements, we can extract the activation energy determined from a thermally activated transport model: $G = G_0 e^{-E_a/k_b T}$, where E_a is the activation energy, k_b is the Boltzmann constant, and G_0 is the temperature-dependent parameter. An Arrhenius plot of the channel conductance and the extracted activation energy for different gate voltages are shown in Figure 4(c). We extracted the Schottky barrier height for charge carrier injection at the flat band condition to be $\Phi_{SB} \sim 70$ meV, which was found at the point where the activation energy deviates from a linear trend indicating that tunneling beings to dominate carrier

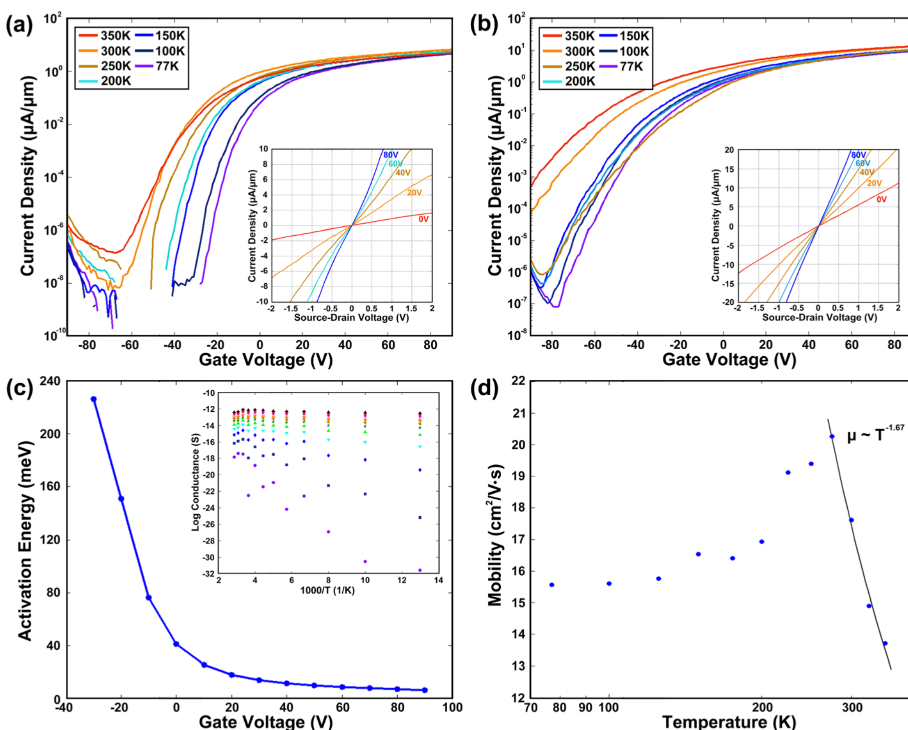

FIG. 4. Temperature-dependent I_{DS}-V_{GS} taken at $V_{DS} = 500$ mV on a transferred monolayer MoS_2 device both before (a) and after (b) passivation with an ALD Al_2O_3 dielectric; insets show room temperature I_{DS}-V_{DS} characteristics as a function of gate voltage. Activation energy as a function of gate voltage; inset shows Arrhenius plot of channel conductance (c). Temperature-dependent mobility for unpassivated devices (d).

injection, matching well with previous reports on exfoliated devices with Ti/Au contacts.[2,14,40] Finally, we show temperature-dependent mobility measurements for our devices in Figure 4(d) using the four-point technique, showing a peak mobility of 20.25 cm^2/V s at 225 K. In the high-temperature transport regime, this data is expected to follow a phonon-limited model, i.e., $\mu \sim T^{-\gamma}$ where $\gamma = 1.69$ according to theoretical calculations. Our experimental results are very close in agreement with this value ($\gamma = 1.67$) which is also in very good agreement with other recent experimental work on exfoliated MoS_2.[14,33] At lower temperatures, the mobility decreases, indicating that the transport in this regime is limited by charged impurity scattering. While this trend has been observed previously on exfoliated samples as well, deposition of a high-κ top gate has been found to screen the effect of coulomb scattering as well as reduce γ through quenching of the homopolar phonon mode.[14]

To summarize, we have characterized back-gated transistors based on chemically synthesized MoS_2 that was grown directly on Si/SiO_2 substrates at elevated temperatures as well as transferred to a new, identical substrate. The results were compared to exfoliated MoS_2 devices that were fabricated and tested using the same procedure. We have shown that there is an intrinsic tensile strain which occurs in the MoS_2 during the growth process as well as residual contamination at the sample interface that can be removed by subsequent transfer; however, this processes results in substantial n-type doping of the sample. The transfer results in monolayer MoS_2 films that have properties comparable or superior to that of mechanically exfoliated MoS_2, both in terms of Raman/PL spectroscopy and field-effect mobility. Furthermore, via temperature-dependent transport measurements we were able to extract scattering constants and the activation energy for transferred MoS_2. We found that our values were in excellent agreement with theoretical predictions and experimental values taken on exfoliated material, suggesting that the currently practiced CVD techniques are capable of producing high quality films.

M.A., M.L.C., A.L.M., R.A.B., and M.D. acknowledge the support of the U.S. Army Research Lab (ARL) Director's Strategic Initiative (DSI) program on interfaces in stacked 2D atomic layered materials. The authors would also like to thank Dr. Pani Varanasi of the Army Research Office for his in-depth technical discussion on 2D atomic layers R&D. S.N., P.M.A., and J.L. acknowledge the support by the Welch Foundation Grant C-1716, NSF Grant DMR-1327093, the U.S. Army Research Office MURI Grant W911NF-11-1-0362, the U.S. Office of Naval Research MURI Grant N000014-09-1066, and the Nanoelectronics Research Corporation Contract S201006.

[1]S. Z. Butler, S. M. Hollen, L. Cao, Y. Cui, J. A. Gupta, H. R. Gutiérrez, T. F. Heinz, S. S. Hong, J. Huang, A. F. Ismach, E. Johnston-Halperin, M. Kuno, V. V. Plashnitsa, R. D. Robinson, R. S. Ruoff, S. Salahuddin, J. Shan, L. Shi, M. G. Spencer, M. Terrones, W. Windl, and J. E. Goldberger, ACS Nano **7**, 2898 (2013).
[2]A. Ayari, E. Cobas, O. Ogundadegbe, and M. S. Fuhrer, J. Appl. Phys. **101**, 014507 (2007).
[3]G.-H. Lee, Y.-J. Yu, X. Cui, N. Petrone, C.-H. Lee, M. S. Choi, D.-Y. Lee, C. Lee, W. J. Yoo, K. Watanabe, T. Taniguchi, C. Nuckolls, P. Kim, and J. Hone, ACS Nano **7**, 7931 (2013).
[4]M. S. Choi, G.-H. Lee, Y.-J. Yu, D.-Y. Lee, S. H. Lee, P. Kim, J. Hone, and W. J. Yoo, Nat. Commun. **4**, 1624 (2013).
[5]K. Roy, M. Padmanabhan, S. Goswami, T. P. Sai, S. Kaushal, and A. Ghosh, Solid State Commun. **175–176**, 35 (2013).
[6]A. Splendiani, L. Sun, Y. Zhang, T. Li, J. Kim, C.-Y. Chim, G. Galli, and F. Wang, Nano Lett. **10**, 1271 (2010).
[7]K.-A. N. Duerloo, M. T. Ong, and E. J. Reed, J. Phys. Chem. Lett. **3**, 2871 (2012).
[8]D. Sercombe, S. Schwarz, O. D. Pozo-Zamudio, F. Liu, B. J. Robinson, E. A. Chekhovich, I. I. Tartakovskii, O. Kolosov, and A. I. Tartakovskii, Sci. Rep. **3**, 3489 (2013).
[9]G. A. Salvatore, N. Münzenrieder, C. Barraud, L. Petti, C. Zysset, L. Büthe, K. Ensslin, and G. Tröster, ACS Nano **7**, 8809 (2013).
[10]H.-Y. Chang, S. Yang, J. Lee, L. Tao, W.-S. Hwang, D. Jena, N. Lu, and D. Akinwande, ACS Nano **7**, 5446 (2013).
[11]Q. He, Z. Zeng, Z. Yin, H. Li, S. Wu, X. Huang, and H. Zhang, Small **8**, 2994 (2012).
[12]J. Yoon, W. Park, G.-Y. Bae, Y. Kim, H. S. Jang, Y. Hyun, S. K. Lim, Y. H. Kahng, W.-K. Hong, B. H. Lee, and H. C. Ko, Small **9**, 3295 (2013).
[13]M. S. Fuhrer and J. Hone, Nat. Nanotechnol. **8**, 146 (2013).
[14]B. Radisavljevic and A. Kis, Nat. Mater. **12**, 815 (2013).
[15]E. Scalisce, M. Houssa, G. Pourtois, V. Afanas'ev, and A. Stesmans, Nano Res. **5**(1), 43–48 (2012).
[16]N. Ma and D. Jena, Phys. Rev. X **4**, 011043 (2014).
[17]H. Wang, L. Yu, Y.-H. Lee, Y. Shi, A. Hsu, M. L. Chin, L.-J. Li, M. Dubey, J. Kong, and T. Palacios, Nano Lett. **12**, 4674 (2012).
[18]S. Najmaei, Z. Liu, W. Zhou, X. Zou, G. Shi, S. Lei, B. I. Yakobson, J.-C. Idrobo, P. M. Ajayan, and J. Lou, Nat. Mater. **12**, 754–759 (2013).
[19]Y. Yu, C. Li, Y. Liu, L. Su, Y. Zhang, and L. Cao, Sci. Rep. **3**, 1866 (2013).
[20]Y.-H. Lee, L. Yu, H. Wang, W. Fang, X. Ling, Y. Shi, C.-T. Lin, J.-K. Huang, M.-T. Chang, C.-S. Chang, M. Dresselhaus, T. Palacios, L.-J. Li, and J. Kong, Nano Lett. **13**, 1852 (2013).
[21]Y. Hao, M. S. Bharathi, L. Wang, Y. Liu, H. Chen, S. Nie, X. Wang, H. Chou, C. Tan, B. Fallahazad, H. Ramanarayan, C. W. Magnuson, E. Tutuc, B. I. Yakobson, K. F. McCarty, Y.-W. Zhang, P. Kim, J. Hone, L. Colombo, and R. S. Ruoff, Science **342**, 720 (2013).
[22]S. Bae, H. Kim, Y. Lee, X. Xu, J.-S. Park, Y. Zheng, J. Balakrishnan, T. Lei, H. R. Kim, Y. I. Song, Y.-J. Kim, K. S. Kim, B. Ozyilmaz, J.-H. Ahn, B. H. Hong, and S. Iijima, Nat. Nanotechnol. **5**, 574 (2010).
[23]X. Li, Y. Zhu, W. Cai, M. Borysiak, B. Han, D. Chen, R. D. Piner, L. Colombo, and R. S. Ruoff, Nano Lett. **9**, 4359 (2009).
[24]M. Amani, M. L. Chin, A. G. Birdwell, T. P. O'Regan, S. Najmaei, Z. Liu, P. M. Ajayan, J. Lou, and M. Dubey, Appl. Phys. Lett. **102**, 193107 (2013).
[25]W. Wu, D. De, S.-C. Chang, Y. Wang, H. Peng, J. Bao, and S.-S. Pei, Appl. Phys. Lett. **102**, 142106 (2013).
[26]B. Radisavljevic, A. Radenovic, J. Brivio, V. Giacometti, and A. Kis, Nat. Nanotechnol. **6**, 147 (2011).
[27]Y. Zhan, Z. Liu, S. Najmaei, P. M. Ajayan, and J. Lou, Small **8**, 966 (2012).
[28]H. J. Conley, B. Wang, J. I. Ziegler, R. F. Haglund, S. T. Pantelides, and K. I. Bolotin, Nano Lett. **13**, 3626 (2013).
[29]C. Rice, R. J. Young, R. Zan, U. Bangert, D. Wolverson, T. Georgiou, R. Jalil, and K. S. Novoselov, Phys. Rev. B **87**, 081307 (2013).
[30]S. Mouri, Y. Miyauchi, and K. Matsuda, Nano Lett. **13**, 5944 (2013).
[31]J. S. Ross, S. Wu, H. Yu, N. J. Ghimire, A. M. Jones, G. Aivazian, J. Yan, D. G. Mandrus, D. Xiao, W. Yao, and X. Xu, Nat. Commun. **4**, 1474 (2013).
[32]Y. Yoon, K. Ganapathi, and S. Salahuddin, Nano Lett. **11**, 3768 (2011).
[33]K. Kaasbjerg, K. S. Thygesen, and K. W. Jacobsen, Phys. Rev. B **85**, 115317 (2012).
[34]K. S. Novoselov, A. K. Geim, S. V. Morozov, D. Jiang, Y. Zhang, S. V. Dubonos, I. V. Grigorieva, and A. A. Firsov, Science **306**, 666 (2004).
[35]H. Liu, A. T. Neal, and P. D. Ye, ACS Nano **6**, 8563 (2012).
[36]I. Childres, L. A. Jauregui, M. Foxe, J. Tian, R. Jalilian, I. Jovanovic, and Y. P. Chen, Appl. Phys. Lett. **97**, 173109 (2010).
[37]B. W. H. Baugher, H. O. H. Churchill, Y. Yang, and P. Jarillo-Herrero, Nano Lett. **13**, 4212 (2013).
[38]W. Bao, X. Cai, D. Kim, K. Sridhara, and M. S. Fuhrer, Appl. Phys. Lett. **102**, 042104 (2013).
[39]See supplementary material at http://dx.doi.org/10.1063/1.4873680 for additional discussion on growth and fabrication methods, interfacial residue, Raman/PL mapping of exfoliated sample, and optical images of fabricated devices.
[40]S. Das, H. Y. Chen, A. V. Penumatcha, and J. Appenzeller, Nano Lett. **13**, 100–105 (2013).